Lipid Sorting by Ceramide and the Consequences for Membrane Proteins

Beate Boulgaropoulos, Michael Rappolt, Barbara Sartori, Heinz Amenitsch, and Georg Pabst*
Institute of Biophysics and Nanosystems Research, Austrian Academy of Sciences, Graz, Austria

ABSTRACT We mimicked the effect of sphingomyelinase activity on lipid mixtures of palmitoyl-oleoyl-phosphatidylcholine, sphingomyelin, ceramide, and 10 mol % cholesterol. Using x-ray diffraction experiments in combination with osmotic stress we found, in agreement with previous studies, that ceramide induces a coexistence of L_α and L_β domains. A detailed structural analysis of the coexisting domains demonstrated an increase of lipid packing density and membrane thickness in the L_α domains upon increasing overall ceramide levels. This provides evidence for a ceramide-driven accumulation of cholesterol in the L_α domains, in support of previous reports. We further determined the bending rigidities of the coexisting domains and found that the accumulation of cholesterol in the L_α domains stabilizes their bending rigidity, which experiences a dramatic drop in the absence of cholesterol. Deriving experimental estimates for the spontaneous curvature and Gaussian modulus of curvature, we show, using a simple geometric model for ion channels, that in this way changes in the conformational equilibrium of membrane proteins can be kept small.

INTRODUCTION

The organization of membranes into functional platforms (rafts), enabling the assembly of signaling proteins or transbilayer transport (1,2), is of particular interest in membrane research. Regarding lipid architecture, membrane rafts are generally considered to be rich in cholesterol and sphingolipids such as sphingomyelin (SM) (3). Under certain circumstances in the life of a cell (e.g., apoptosis), SM is hydrolyzed to ceramide (Cer) by sphingomyelinease (4,5). This significantly impacts lateral membrane structure (6–8), and it has been speculated that Cer stabilizes membrane rafts (9). In a previous report, performed on mixtures of palmitoyl-oleoyl phosphatidylcholine (POPC), SM, and Cer, we showed that Cer may induce macroscopic phase separation into stable lamellar fluid (L_α) and gel (L_β) domains over a certain range of temperatures and Cer concentrations (10). In that study, we further showed that the phase separation is due to preferential interactions of Cer with SM, such as hydrogen bonding, leading to an enrichment of SM and Cer in the L_β domains and an enrichment of POPC in the coexisting L_α domains. The depletion of SM from the L_α domains causes a fourfold drop in the bending rigidity of the fluid phase (11). This change of membrane elasticity can be coupled to transmembrane protein activity (12,13), and we estimated significant changes in the conformational equilibrium of simple geometric protein models (11).

In this report, we focus on the competition of Cer with cholesterol (Chol) in the context of sphingomyelinase activity, which is mimicked by gradually replacing SM with Cer in mixtures of POPC, SM, and Chol. In particular, we are interested in effects regarding membrane lateral structure and elasticity and their putative consequences for transmembrane protein activity. Cholesterol is abundant in plasma membranes (14) and interacts preferentially with saturated acyl chains as compared to unsaturated hydrocarbon chains (15,16). Therefore, it contends with Cer for SM (17–24). It is also well known that Chol condenses fluid membranes (see, e.g., (25–28)). Several ternary lipid mixtures of Chol mimicking the outer plasma membrane exhibit phase coexistence of liquid ordered (L_o), liquid disordered (L_d), or gel phases (29). Such phase coexistence has been reported also for POPC/SM/Chol, although the form of the phase coexistence regimes and direction of tie lines remain controversial (30,31). Although Chol levels are on the order of 30–50 mol % in plasma membranes (14), we chose an intermediate Chol concentration of 10 mol %. According to Veatch and Keller (31), this system offers the advantage of being just outside a L_o/L_d phase-coexistence regime, and we will thus be able to learn about the competition between Cer and Chol under simplified conditions, i.e., starting from a homogenous mixture. In this concentration range, Cer has been reported to displace Chol from L_o domains (17,19–21,23). In turn, an increase of Chol concentration was found to gradually dissolve Cer-rich gel domains (18,22–24).

In this report, we seek to understand 1), how Chol at intermediate concentrations affects the properties of the Cer-enriched L_β phase and the coexisting L_α phase; and 2), how these properties are coupled to membrane protein activity. For this purpose, we compared our x-ray diffraction results to those of previous studies in the absence of Chol (10,11,32). Osmotic stress experiments showed that the bending rigidity of the L_α phase remains unaffected by L_β-domain formation, which is attributed to the accumulation of Chol in L_α domains. We further estimated the spontaneous curvatures and Gaussian moduli of curvature of the coexisting phases, allowing us to address possible consequences of membrane restructuring for protein function in the case of a simple ion channel. Our calculations showed

Submitted January 11, 2012, and accepted for publication March 23, 2012.

*Correspondence: georg.pabst@oeaw.ac.at

Editor: Heiko Heerklotz.

0006-3495/12/05/2031/8 $2.00

doi: 10.1016/j.bpj.2012.03.059

that Chol minimizes membrane-mediated activity changes of proteins located in the L_α domains that would take place in its absence (11).

MATERIALS AND METHODS

Liposome preparation

POPC, egg-SM, and C16:0-Cer were purchased from Avanti Polar Lipids (Birmingham, AL) and used without further purification. Chol, polyethylene glycol (PEG, molecular mass 8000 g/mol), and all other chemicals (solvents in pro analysi grade) were from Sigma-Aldrich (Castle Hill, Australia).

Lipid stock solutions were prepared by dissolving weighted amounts of dry lipid powder from freshly opened sample containers from the suppliers in chloroform/methanol (2:1, v/v). The appropriate volumes of the stock solutions were mixed and the organic solvent was evaporated at room temperature under a gentle stream of nitrogen. The samples were then placed under vacuum for at least 12 h to form a thin lipid film on the bottoms of glass vials. Multilamellar vesicles (MLVs) were prepared by first suspending the dry lipid films in 18 MΩ/cm water (UHQ PS, USF Elga, Wycombe, UK) at a lipid concentration of 50 mg/ml and then incubating the dispersions for 4 h in the fluid phase of the system with intermittent vigorous vortex mixing. At least eight freeze-thaw circles were performed. For the osmotically stressed samples, the fully hydrated MLVs were prepared at a concentration of 200 mg/ml, as detailed above, and then diluted to 50 mg/ml by a PEG solution of a given concentration whose osmotic pressure was determined using a Knaur (Berlin, Germany) vapor-pressure osmometer. The sample was equilibrated at a given osmotic pressure for at least 2 days.

Small and wide-angle x-ray diffraction

Synchrotron small- and wide-angle x-ray diffraction experiments were performed at the Austrian SAXS beamline at Elettra (Trieste, Italy) (33,34) using a photon energy of 8 keV. SAXD patterns were recorded in a q-range of 2.67×10^{-4} – 0.95 $Å^{-1}$ ($q = 4\pi/\lambda \sin\theta$) using a mar300-image-plate detector (Marresearch, Norderstedt, Germany). Integration of scattered intensity and primary data reduction were performed using the program Fit2D. WAXD patterns (q-range = 0.77 – 2.79 $Å^{-1}$), were recorded simultaneously using a Gabriel-type PSD. Samples were contained in 1-mm quartz-glass capillaries at a distance of 1.121 m to the image-plate detector. Before measurements, samples were equilibrated at 37°C for at least 10 min, using a circulating water bath (Unistat CC, Huber, Offenburg, Germany). Typical exposure times were 300 s. The instrumental resolution was determined to have a full width at half-maximum of $\delta q = 2.23 \times 10^{-3}$ $Å^{-1}$.

Lamellar repeat distances, d, were derived from a Lorentzian fit to the first-order Bragg peaks. From the peaks, we derived the bilayer electron density profiles using standard techniques as reported previously (11). Further, we used the same definition for the membrane thickness $d_B = d_{HH} + 10$ Å (d_{HH} is the distance between the two maxima of the electron-density profile).

Hydrocarbon chain positional correlation peaks occur in the WAXD regime. Peaks of the coexisting phases were fitted with two Lorentzians (Fig. S1 in the Supporting Material). For Cer = 30 mol % and 35 mol %, additional sharp peaks appeared that required additional Lorentz peak functions in the analysis. The L_β phase is characterized by a single sharp peak occurring at $q_{11} \sim 1.51$ $Å^{-1}$. From the peak position, we calculated, as previously, the lateral area/lipid $A = 16\pi^2/(\sqrt{3}q_{11}^2)$. The chain correlations of the L_α phase exhibit a broad peak at $q_0 \sim 1.40$ $Å^{-1}$. Unlike the long-range order present in the L_β phase, hydrocarbons in the L_α phase are fluid and exhibit short-range order. It has been shown (35), that the average chain separation can then be calculated using $a = 9\pi/4q_0$. The decay constant of the short-range positional correlations was derived from $\xi = 2/\Delta q_{0corr}$ (35), using the corrected full width at half-maximum of the chain correlation peak.

Osmotic stress experiments and analysis

Osmotic pressure experiments combined with SAXD were performed as described previously using PEG 8000 (11). In the analysis of the isotherms, we considered van der Waals attraction, hydration repulsion, and repulsion due to bilayer bending fluctuations. The osmotic pressure, Π, is equated with the sum of disjoining pressures that results from these interactions, i.e., $\Pi = P_{vdW} + P_{hyd} + P_{flug}$ using the same forms for the van der Waals pressure, P_{vdW}, hydration pressure, P_{hyd}, and fluctuation pressure, P_{fluc}, as reported previously (11). Parameters of P_{vdW} are the Hamaker constant, H, and the membrane thickness, d_B. The latter parameter is determined from SAXD (see above). For the Hamaker constant, we choose the theoretical value $H = 4.3 \times 10^{-21}$ J (36), as applied in previous studies from our laboratory (11,37). Parameters of hydration interactions are the empirical scaling constant, P_h, and the decay constant, λ_h. Fluctuation interactions were only considered for fluid phases. The presently used form of P_{fl} contains P_h, λ_h, and, in particular, the bending rigidity, K_C, as adjustable parameters. As described previously (11,37), the isotherms were fitted iteratively, starting with the analysis of data with $\Pi > 1$ atm and a constrained estimate for K_C. K_C was subsequently adjusted in a fit of the full isotherm, returning with this new value of K_C to Step 1 of the analysis, until the fit to the osmotic pressure data could not be improved any further.

Calculation of effects on transmembrane proteins

Bulk elastic properties of membrane lipids may affect the conformational equilibrium of membrane proteins (12,13,38). The basic idea is that conformational changes of proteins that go hand in hand with changes in the cross-sectional area, ΔA, need to take place against a distribution of repulsive and attractive intramembrane pressures, p, known as the lateral-pressure profile. Take, for example, the opening of an ion channel, which involves the opening of a passage for ions, i.e., the transition from a closed (r) to an open state (t). The thermodynamic equilibrium can be described by a distribution of closed to open channels $K_0 = [r_0]/[t_0]$. Changes in the distribution of lateral pressures, e.g., upon changes in lipid composition due to sphingomyelinase activity, will also change the conformational equilibrium (39), which is then given by $K = [r]/[t]$. It can be shown that the two equilibria are related by $K = K_0 \exp(\alpha)$, with $\alpha = \int \Delta p(z)\Delta A(z)dz/k_BT$ being the change of work associated with the opening of the channel in the changed lateral-pressure field (40).

For simple geometric shapes of proteins, α, and hence K/K_0, can be calculated analytically (40). In the case of hourglass-shaped proteins, consisting of an n-mer of bent helices, we recently showed that $\alpha = 2\pi[(2r_{max}\Delta\tan\varphi - d_B\Delta\tan^2\varphi)\Delta P_1 + \Delta\tan^2\varphi\Delta P_2]/k_BT$ (11,41), where r_{max} is the outer radius of the protein at the position of the lipid headgroups, φ the opening angle of the pore, and ΔP_1 and ΔP_2 the changes in the first and second integral moments of the lateral-pressure profile imposed in this case upon the addition of Cer. The two integral moments are related to membrane elasticity by (42) $P_1 = \kappa_m c_0$ and $P_2 = \kappa_G$, where κ_m is the monolayer bending rigidity, c_0 the spontaneous curvature, and κ_G the Gaussian modulus of curvature. These parameters can be determined from experiment. In particular, $\kappa_m = K_C/2$ is derived from osmotic pressure experiments described above. We further derived c_0 by measuring lipids in the inverted hexagonal phase (43) (see Supporting Material). κ_G was estimated using $\kappa_G \sim -0.8\ \kappa_m$ (13).

RESULTS

Structural properties of coexisting fluid and gel domains

Fig. 1 shows the SAXD and WAXD patterns of fully hydrated MLVs at 37°C. Bilayers were initially composed of POPC/SM/Chol (45:45:10); subsequently, SM was

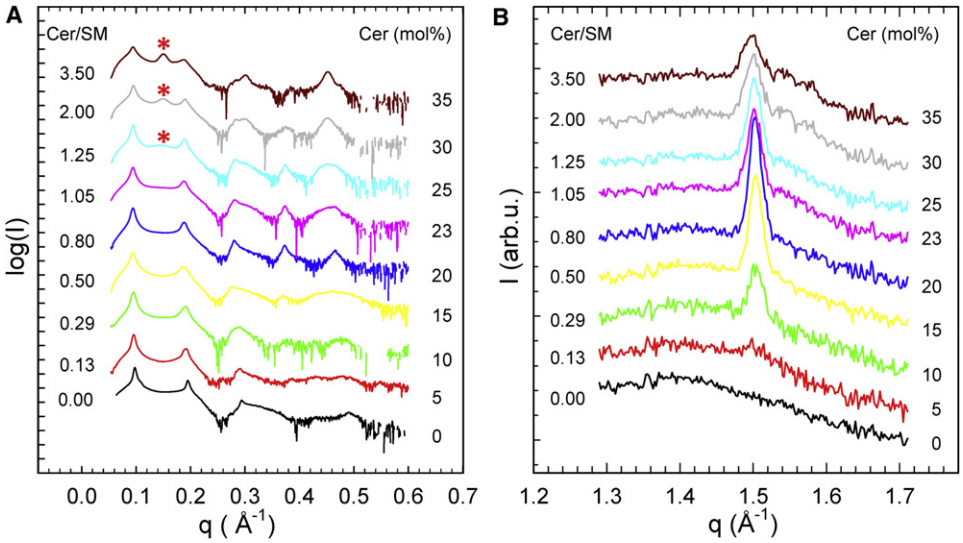

FIGURE 1 Changes in scattering patterns (panel *A*, SAXD; panel *B*, WAXD) of MLVs composed of POPC/SM/Chol upon replacing SM gradually with Cer. Asterisks in *A* indicate the position of the first diffraction order of the Cer phase.

gradually substituted by Cer in the concentration range from 0 to 35 mol %. SAXD patterns up to 23 mol % Cer were characteristic for a single lamellar phase. However, the sharp peak on top of a diffuse peak observed in the WAXD regime in the presence of Cer clearly demonstrates the coexistence of L_α and L_β domains. The observation of a single *d*-value for coexisting phases may have several reasons, some of which are detailed in Mills et al. (44). For example, like domains may not be in registry, or they may happen to have similar *d*-values, i.e., the smaller d_B of L_α and larger d_B of L_β phases, is compensated by a larger bilayer separation, $d_W = d - d_B$ for L_α and smaller d_W for L_β. Phase coexistence in the SAXD regime will be revealed upon the application of osmotic pressure (see below). However, to differentiate between different domain alignments in MLVs is not within the scope of this work. For Cer concentrations $\geq$25 mol %, SAXD patterns showed an additional peak with $d = 41.9$ Å, which became increasingly prominent with Cer concentration. The *d*-value is comparable to that reported previously for pure Cer phases (10,32,45) and signifies the formation of Cer crystallites, which are insoluble in the lipid membrane. Precipitation of Cer crystallites was also observed as a decrease of the L_β chain correlation peak intensity and the formation of higher *q* satellite peaks (Fig. 1 *B*). Concentrations of 25 mol % Cer correspond to a Cer/SM molar ratio of 1.25. Thus, as soon as the Cer level increases over that of SM, any additional Cer cannot be integrated into the lipid bilayer but forms a crystalline-like precipitate. In the absence of Chol, Cer precipitates at significantly higher concentrations (35 mol %) (10,32).

As a next step, we performed a detailed analysis of the WAXD data, in comparison to previously published data that did not contain Chol (10). This is facilitated by plotting all structural parameters as a function of the Cer/SM molar ratio. We first focus on the L_β domains using the data analysis described in the Materials and Methods section. The area/lipid, *A*, of the gel domains exhibited a value of 40.3 Å^2 at the lowest Cer concentration, decreased slightly at Cer/SM = 0.3, and then increased linearly by ~0.3 Å^2 toward higher Cer/SM ratios (Fig. 2). The increase of *A* for Cer/SM $\geq$ 0.29 is most likely due to the splay induced by the spontaneous curvature of Cer (see Supporting Material). In the absence of Chol, *A* increased over the entire range of Cer concentrations studied. Differences in absolute *A*-values in the absence and presence of Chol show that lipid compositions of the domains differ. Most likely, this is due to Chol partitioning into the L_β domains. In general, the overall extent of area variation is much more pronounced in the absence of Chol. Thus, the difference between the area/lipid of Chol-containing and that of Chol-free bilayers decreases with Cer content, which could indicate a displacement of Chol from the gel domains, as described in reports of previous studies that used different experimental techniques (17,19–21,23).

A consequence of this scenario would be that Chol accumulates in the L_α domains. Since Chol is well known for its

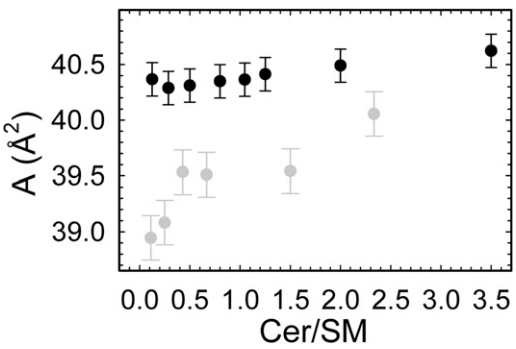

FIGURE 2 Comparison of lateral area/lipid of L_β domains in the presence (*black circles*) and absence (*gray circles*) of Chol (10) as a function of the Cer/SM molar ratio.

membrane-condensing effect (see e.g., Hodzic et al. (27)), we expect to observe changes of the corresponding broad WAXD peak. Indeed, the average distance between the acyl chains in the L_α domains provides clear evidence for such a scenario (Fig. 3). In the Cer/SM range 0–1.25, the distance a decreased quasilinearly and then remained constant toward higher Cer concentrations. The change in the slope of a coincided with the solubility limit of Cer in this system. Thus, Chol accumulates in the L_α phase, as long as Cer is able to form an L_β phase with SM (Cer/SM $\leq$ 1). This leads to an increase of packing density in L_α because of the significantly smaller lateral area/molecule of Chol (46) as compared to SM (47) and due to the umbrella effect of POPC (26). At the same time, the decay of the positional correlations did not show significant changes, with an average value of $\xi = 5.4$ Å. This is a typical value for fluid hydrocarbons (35) and demonstrates that Chol accumulation in the L_α domains does not affect the short-range order of the acyl chains.

Membrane thickness and domain elasticity from osmotic stress experiments

We performed SAXD experiments under osmotic stress, as described previously in detail (11). Fig. 4 *A* shows the SAXD patterns for Cer/SM = 0 and Cer/SM = 0.5 at mild osmotic pressure (Π = 1.31 atm). In the presence of Cer, this pressure was sufficient to reveal the two lamellar lattices of the L_α and L_β phase. Only a single set of lamellar peaks, and hence no coexistence of L_o and L_d domains, was observed in the initial POPC/SM/Chol mixture. Also, application of higher osmotic pressures and lowering sample temperature to 10°C did not reveal the coexistence of macroscopically stable L_o and L_d domains (Fig. S3). Note that for the Chol concentration studied here, this is in agreement with a previous fluorescence microscopy study (31). There is a small, but distinct, difference from the compositional phase diagram based on fluorescence spectroscopy (30), where 10 mol % Chol would be just within a L_o/L_d coexistence regime. However, as discussed previously (10,29,48), this difference could be due to using egg-SM (here) instead of palmitoyl-SM (30), or different experimental windows of the applied techniques. Further, there are subtle differences between stable and unstable lipid domains, as well as macroscopic and nanoscopic domains, which can be discerned only upon the application of different experimental techniques (10,48). Note that we recently observed phase coexistence in the same system at higher Chol concentrations (to be published in a separate report). Thus, x-rays are sensitive to phase coexistence in POPC/SM/Chol.

From the SAXD patterns shown in Fig. 4 *A*, we were able to derive the electron-density profiles and the corresponding membrane thicknesses, d_B, as described previously (11). Results are shown in Fig. 4 *B* and Table 1, which, to facilitate a comparison with other reports, also includes the headgroup-to-headgroup distances, d_{HH}. In the absence of Cer, we found a membrane thickness of $d_B = 49.5 \pm 0.2$ Å, which is 1.1 Å larger than our previously reported value in the absence of Chol (11). The increase of d_B goes hand in hand with the bilayer condensation by Chol, as reported previously for several lipid/ Chol mixtures (see, e.g., Hodzic

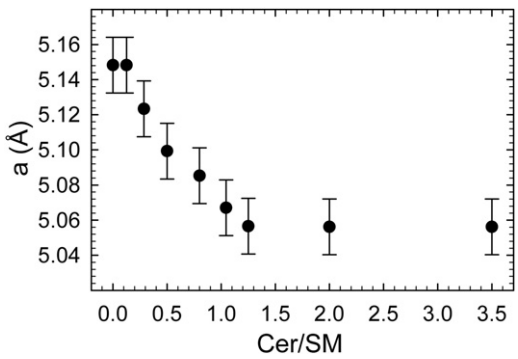

FIGURE 3 Average distance between acyl chains in the L_α domains as a function of Cer concentration.

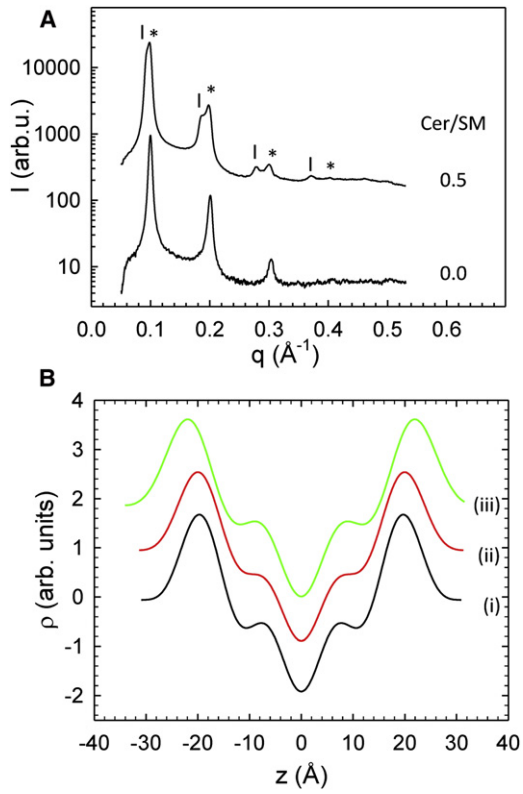

FIGURE 4 (*A*) SAXD patterns of osmotically stressed MLVs (Π = 1.31 atm) in the presence and absence of Cer. Two lamellar phases (L_α (*) and L_β (|)) are observed for Cer/SM = 0.5. (*B*) The corresponding electron-density profiles derived from the peak intensities. Profiles shown are for POPC/SM/Chol (i), the L_α phase of POPC/SM/Chol (ii), and the coexisting L_β domains (iii).

TABLE 1 Structural and interaction parameters

Cer (mol %)	Phase	d_B (Å)	d_{HH} (Å)	P_h (atm)	λ_h (Å)	K_c (k_BT)
0	L_α	49.5	39.5	4555	1.51	78.9
10	L_α	50.2	40.2	4627	1.51	77.3
10	L_β	54.1	44.1	1.38×10^4	1.51	>100

Data were derived from osmotic isotherms of POPC/SM/Chol (45:45:10) and the coexisting L_α/L_β domains of POPC/SM/Cer/Chol (45:30:15:10). K_C was not measured for L_β domains. We give a lower limit instead.

et al. (27).). In the presence of Cer (Cer/SM = 0.5), we found $d_B = 50.2 \pm 0.2$ Å for the L_α domains and $d_B = 54.1 \pm 0.2$ Å for the coexisting L_β domains. Naturally, the gel phase shows the largest membrane thickness due to the all-*trans* conformations of the hydrocarbon chains. Interestingly, also the d_B of the coexisting L_α phase is larger than the membrane thickness of the non-phase-separated system (Cer/SM = 0). This supports the above-discussed scenario in which Cer leads to accumulation of Chol in the L_α phase, as additional Chol will also increase d_B (see e.g., Hodzic et al. (27).). In the absence of Chol, the d_Bs of the L_α phases were found to be comparable (11).

Accumulation of Chol in the L_α domains certainly has significant consequences for the elasticity of coexisting phases. This can be probed by variation of the osmotic pressure in combination with SAXD. Fig. 5 shows the osmotic pressure data in the presence of Chol. At the highest Π measured, hydration repulsion dominated the disjoining pressures. As Π was decreased, fluctuation repulsion, which has a larger decay constant, became more and more prominent. Finally, we observed a typical deviation from linearity in the semilogarithmic plot, which is when van der Waals attraction between the bilayers comes into play and the bilayers obtain their equilibrium separation. Visual inspection of the data presented in Fig. 5 shows that the equilibrium separation of the L_β domains obtained at $\Pi = 0$ is significantly smaller than that of the L_α phases. This is characteristic for gel phases, where repulsion from bending fluctuations plays no role. Further, the two isotherms for the fluid phases are practically identical. Thus, we expect that all adjustable interaction parameters of the L_α phase of POPC/SM/Chol, including the bending rigidity, will not change significantly upon the addition of Cer. Indeed, all values for the interaction parameters P_h, λ_h, and K_C obtained from fits to the osmotic pressure data agree within experimental error (Table 1). Compared to our previous study in the absence of Chol, the K_C of the fluid domains is ~34% larger (11). This effect is typical for the condensing abilities of Chol in fluid lipid bilayers (28,49).

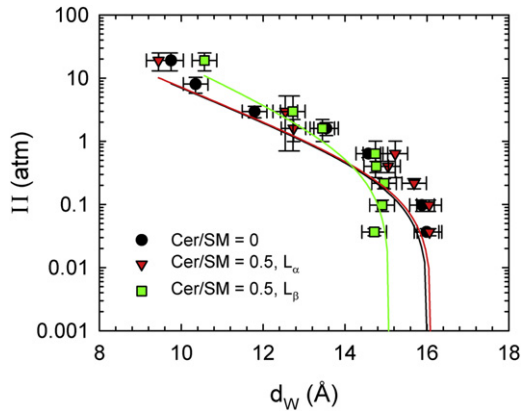

FIGURE 5 Equation of state for POPC/SM/Chol (45:45:10) (*circles*) and for the L_α domains (*triangles*) and L_β domains (*squares*) of POPC/SM/Cer/Chol (45:30:15:10). Solid lines correspond to fits.

DISCUSSION

Compared to our previous study (10), Cer precipitated at significantly lower concentrations (Fig. 1). Thus, the competition between Chol and Cer lowers the solubility of Cer in the bilayer. Our analysis of the WAXD data of the L_β domains showed that the difference in lateral area/lipid between samples containing and those not containing Chol decreased with increasing Cer concentration (Fig. 2). Previously, we demonstrated by infrared spectroscopy preferential interactions between Cer and SM, leading to the formation of the gel phase (10). We assume that this is also the case in the presence of Chol, which is further supported by mass spectroscopy data (50). However, because of preferential interactions of Chol with saturated hydrocarbons (15,16), Chol will also partition into the L_β domains, explaining the observed differences in A (Fig. 2). The decrease of this difference with increasing Cer content then suggests that Chol would be depleted from the L_β domains and consequently accumulate in the L_α domains, in agreement with observations by others (17,19–21,23). This scenario is strongly supported by our WAXD analysis of the L_α domains, showing increased packing density as Cer levels are increased. Furthermore, the increase in d_B of the L_α domains (Table 1) also agrees with increased Chol levels. In the absence of Chol, we observed previously an almost fourfold decrease of the bending rigidity of the L_α domains, which was explained by the depletion of SM from the fluid phase due to SM/Cer interactions (11). In this study, no significant changes in K_C could be detected upon the addition of Cer (Table 1). Thus, Chol accumulation in the L_α domains recovers the drop in K_C by depletion of SM from the fluid phase.

As a secondary effect, Chol accumulation in the L_α domains seems also to constrain POPC to the L_α domains. At Cer/SM = 1, all pairwise interactions between Cer and SM are saturated. Nonetheless, we were able to solubilize an additional amount of ~5 mol % Cer in the bilayers in the absence of Chol (10). This was explained by the incorporation of some limited amounts of POPC in L_β domains (32), which has a lower affinity for Cer than SM but still

displays L_β domains in binary mixtures with Cer (20). In the presence of Chol, we observed Cer crystallites as soon as Cer/SM > 1 (Fig. 1). This significantly lower solubility of Cer therefore suggests that POPC is not able to partition into the L_β domains for Cer/SM > 1 but remains within the L_α domains, most likely due to preferred interactions with Chol as compared to Cer.

Potential effects on ion channels

It is instructive to ask how these changes in bulk membrane properties may affect the activity of membrane proteins. It is well known that changes in the distribution of lateral pressure are linked to protein function (12,13). In a previous study, based on the drop in K_C in the L_α phase in the absence of Chol, we calculated possible consequences for the activity of channel proteins with hourglass-shaped geometry as a function of pore size (11). Since K_C does not change significantly in this scenario, one could argue that protein activity will not be affected at all. However, in addition to K_C, protein activity is also linked to the spontaneous curvature, c_0, and the Gaussian modulus of curvature, κ_G (13).

It is not possible to measure the c_0 for coexisting phases. However, c_0 can be estimated from the molecular-mass sum of the c_0s of the individual lipid components of a given phase (51). Of all the lipids used in this study, c_0 has been reported only for Chol, where it was found to be between -0.036 Å^{-1} and -0.043 Å^{-1} (52). We thus decided to measure the spontaneous curvatures of all presently used lipids using a recently refined procedure (43). Details can be found in the Supporting Material. We arrive at $c_0 = -0.003$ Å^{-1} for both SM and POPC, which is close to 0, as expected from their preference for forming lamellar phases. Further, $c_0 = -0.031$ Å^{-1} for Cer, and $c_0 = -0.038$ Å^{-1} for Chol. The latter value agrees well with previously published data (see above). To determine the c_0s of the coexisting lipid phases, exact knowledge of the lipid composition of the individual domains is required. This is presently not available. However, for this discussion it is sufficient to consider the extreme cases in lipid sorting by Cer. Henceforth, we assume that in the absence of Chol, the L_α domains are composed of POPC only, whereas the coexisting L_β domains contain an equimolar mixture of SM and Cer. In the presence of 10 mol % Chol, the L_α domains, in turn contain all POPC and all Chol, i.e., POPC/Chol = 0.815/0.185, whereas the L_β phase is again given by SM/Cer = 1. Further, our calculation of c_0 implicitly assumes random mixing of the lipids within a given domain, which should be fulfilled, neglecting boundary effects.

Table 2 shows the resulting spontaneous curvatures for these domain compositions. It is clear that the L_β domains exhibit the largest negative value for spontaneous curvature due to the high concentration of Cer. Also, the presence of Chol in the L_α domains leads to a significant increase of c_0. The monolayer bending rigidities were calculated from the measured K_C values assuming that differences in lipid composition between experiment and those reported in Table 2 do not affect the κ_ms significantly. Gaussian moduli of curvature were estimated as detailed in the previous section.

TABLE 2 Spontaneous curvature, monolayer bending rigidity, and Gaussian modulus of curvature for POPC/SM/Cer mixtures in the presence and absence of Chol

Lipid system	Domain	Phase	Molar ratio	c_0 (10^{-2} Å^{-1})	κ_m (k_BT)	κ_G (k_BT)
POPC/SM	—	L_α	0.5:0.5	−0.314	28.9	−23.1
POPC/SM/Cer	POPC	L_α	1	−0.326	7.9	−6.3
	SM/Cer	L_β	0.5:0.5	−3.41	~50	−40
POPC/SM/Chol		L_α	0.45:0.45:0.1	−0.662	39.5	−31.6
POPC/SM/Cer/Chol	POPC/Chol	L_α	0.815:0.185	−0.967	38.7	−30.9
	SM/Cer	L_β	0.5:0.5	−3.41	~50	−40

With these data, we calculated the changes in first and second integral moments of the lateral pressure profile, ΔP_1 and ΔP_2, due to lipid sorting by Cer. The results reported in Table 3 show that both L_α domains exhibit positive changes in ΔP_1 and ΔP_2, regardless of the presence or absence of Chol. This signifies a shift of lateral pressure toward the lipid/water interface (11,12). The effect is more pronounced in the absence of Chol, in agreement with previous theoretical work on lipid mixtures showing that Chol shifts lateral pressure toward the membrane interior (39). In turn, ΔP_1 and ΔP_2 are negative for the L_β domains, implying a redistribution of lateral pressure toward the bilayer center.

Next, it is interesting to consider the effect of these changes on transmembrane proteins, e.g., the opening probability of ion channels. For these calculations, we chose an hourglass-shaped channel protein with the same geometry parameters listed previously (41). Table 3 reports the changes of work, α, to open the ion channel in the changed lateral-pressure field. Negative values of α indicate a shift of the conformational equilibrium toward open channels, and conversely, positive α values signify channel closing. Thus, ion channels in the L_α domains will have increased probability of being in an open state, whereas those located on L_β domains will be inhibited. Inhibition of protein

TABLE 3 Effects on hourglass-shaped ion channels

	Phase	ΔP_1 (k_BT/Å)	ΔP_2 (k_BT)	α	K/K_0	
POPC/SM/Cer	L_α	0.062	16.8	−7.7	4.5×10^{-4}	↑
	L_β	−0.31	−16.9	18.3	9.3×10^{7}	↓
POPC/SM/Cer/Chol	L_α	0.005	0.64	−0.4	6.5×10^{-1}	↑
	L_β	−1.16	−8.4	55.1	8.7×10^{23}	↓

Changes of first and second integral moments, P_1 and P_2, of the lateral-pressure profiles and the consequences for conformational equilibria K/K_0. Up and down arrows indicate shifts toward channel opening and channel closing, respectively.

function in gel phases is a well-known fact. We therefore focus on the effects within the L_α domains and in particular on K/K_0 (Table 3), which expresses the magnitude of the shifts of conformational equilibrium. Both L_α phases show a decrease of closed states. However, the effect is much less expressed in the presence of Chol, where the number of open states increases by a factor of ~1.5, as compared to ~2000 when no Chol is present.

SUMMARY AND CONCLUSIONS

We have performed a comprehensive structural analysis of POPC/SM/Chol/Cer mixtures with 10 mol % Chol and compared our results to structural data reported in the absence of Chol (10,11,32). Upon gradually substituting SM with Cer, we found, in particular, 1), a decrease in the difference in lateral area/lipid in the L_β domains of Chol-free membranes; 2), tighter lipid packing in the L_α domains; and 3), an increase in the membrane thickness of the L_α domains. In support of previous studies (17,19–21,23), this provides evidence that competition between Cer and Chol leads to an accumulation of Chol in L_α domains. Theoretical calculations of the effects of ion channel activity showed that channel opening in the L_α domains occurs with a significantly higher probability in the absence of Chol. This highlights the important role of Chol in maintaining membrane stability and function. In the absence of Chol, lipid sorting by Cer induces strong shifts of the conformational equilibrium of ion channels in L_α domains toward open states, which could be detrimental to cell function and may interfere with the controlled disposal of cells during apoptosis. In the presence of Chol, these changes are much more moderate and can possibly be more easily handled.

SUPPORTING MATERIAL

Determination of spontaneous curvatures, phase separation in POPC/SM/Chol, three figures, a table, and references (53–60) are available at http://www.biophysj.org/biophysj/supplemental/S0006-3495(12)00400-6.

REFERENCES

1. Lingwood, D., and K. Simons. 2010. Lipid rafts as a membrane-organizing principle. *Science.* 327:46–50.
2. Simons, K., and J. L. Sampaio. 2011. Membrane organization and lipid rafts. *Cold Spring Harb. Perspect. Biol.* 3:a004697.
3. Pike, L. J. 2006. Rafts defined: a report on the Keystone Symposium on Lipid Rafts and Cell Function. *J. Lipid Res.* 47:1597–1598.
4. van Blitterswijk, W. J., A. H. van der Luit, …, J. Borst. 2003. Ceramide: second messenger or modulator of membrane structure and dynamics? *Biochem. J.* 369:199–211.
5. Andrieu-Abadie, N., and T. Levade. 2002. Sphingomyelin hydrolysis during apoptosis. *Biochim. Biophys. Acta.* 1585:126–134.
6. Goñi, F. M., and A. Alonso. 2006. Biophysics of sphingolipids I. Membrane properties of sphingosine, ceramides and other simple sphingolipids. *Biochim. Biophys. Acta.* 1758:1902–1921.
7. Cremesti, A. E., F. M. Goni, and R. Kolesnick. 2002. Role of sphingomyelinase and ceramide in modulating rafts: do biophysical properties determine biologic outcome? *FEBS Lett.* 531:47–53.
8. Kolesnick, R. N., F. M. Goñi, and A. Alonso. 2000. Compartmentalization of ceramide signaling: physical foundations and biological effects. *J. Cell. Physiol.* 184:285–300.
9. Goñi, F. M., and A. Alonso. 2009. Effects of ceramide and other simple sphingolipids on membrane lateral structure. *Biochim. Biophys. Acta.* 1788:169–177.
10. Boulgaropoulos, B., Z. Arsov, …, G. Pabst. 2011. Stable and unstable lipid domains in ceramide-containing membranes. *Biophys. J.* 100: 2160–2168.
11. Pabst, G., B. Boulgaropoulos, …, P. Laggner. 2009. Effect of ceramide on nonraft proteins. *J. Membr. Biol.* 231:125–132.
12. Cantor, R. S. 1997. Lateral pressures in cell membranes: a mechanism for modulation of protein function. *J. Phys. Chem. B.* 101:1723–1725.
13. Marsh, D. 2007. Lateral pressure profile, spontaneous curvature frustration, and the incorporation and conformation of proteins in membranes. *Biophys. J.* 93:3884–3899.
14. van Meer, G., D. R. Voelker, and G. W. Feigenson. 2008. Membrane lipids: where they are and how they behave. *Nat. Rev. Mol. Cell Biol.* 9:112–124.
15. Silvius, J. R. 2003. Role of cholesterol in lipid raft formation: lessons from lipid model systems. *Biochim. Biophys. Acta.* 1610:174–183.
16. Ramstedt, B., and J. P. Slotte. 2006. Sphingolipids and the formation of sterol-enriched ordered membrane domains. *Biochim. Biophys. Acta.* 1758:1945–1956.
17. Megha, and E. London. 2004. Ceramide selectively displaces cholesterol from ordered lipid domains (rafts): implications for lipid raft structure and function. *J. Biol. Chem.* 279:9997–10004.
18. Fidorra, M., L. Duelund, …, L. A. Bagatolli. 2006. Absence of fluid-ordered/fluid-disordered phase coexistence in ceramide/POPC mixtures containing cholesterol. *Biophys. J.* 90:4437–4451.
19. Chiantia, S., N. Kahya, …, P. Schwille. 2006. Effects of ceramide on liquid-ordered domains investigated by simultaneous AFM and FCS. *Biophys. J.* 90:4500–4508.
20. Silva, L. C., R. F. de Almeida, …, M. Prieto. 2007. Ceramide-domain formation and collapse in lipid rafts: membrane reorganization by an apoptotic lipid. *Biophys. J.* 92:502–516.
21. Sot, J., M. Ibarguren, …, A. Alonso. 2008. Cholesterol displacement by ceramide in sphingomyelin-containing liquid-ordered domains, and generation of gel regions in giant lipidic vesicles. *FEBS Lett.* 582:3230–3236.
22. Staneva, G., C. Chachaty, …, P. J. Quinn. 2008. The role of sphingomyelin in regulating phase coexistence in complex lipid model membranes: competition between ceramide and cholesterol. *Biochim. Biophys. Acta.* 1778:2727–2739.
23. Castro, B. M., L. C. Silva, …, M. Prieto. 2009. Cholesterol-rich fluid membranes solubilize ceramide domains: implications for the structure and dynamics of mammalian intracellular and plasma membranes. *J. Biol. Chem.* 284:22978–22987.
24. Staneva, G., A. Momchilova, …, K. Koumanov. 2009. Membrane microdomains: role of ceramides in the maintenance of their structure and functions. *Biochim. Biophys. Acta.* 1788:666–675.
25. Mouritsen, O. G., and K. Jørgensen. 1994. Dynamical order and disorder in lipid bilayers. *Chem. Phys. Lipids.* 73:3–25.
26. Huang, J., and G. W. Feigenson. 1999. A microscopic interaction model of maximum solubility of cholesterol in lipid bilayers. *Biophys. J.* 76:2142–2157.
27. Hodzic, A., M. Rappolt, …, G. Pabst. 2008. Differential modulation of membrane structure and fluctuations by plant sterols and cholesterol. *Biophys. J.* 94:3935–3944.
28. Khelashvili, G., M. Rappolt, …, D. Harries. 2011. Impact of sterol tilt on membrane bending rigidity in cholesterol and 7-DHC containing DMPC membranes. *Soft Matter.* 7:10299–10312.

29. Marsh, D. 2009. Cholesterol-induced fluid membrane domains: a compendium of lipid-raft ternary phase diagrams. *Biochim. Biophys. Acta.* 1788:2114–2123.

30. de Almeida, R. F., A. Fedorov, and M. Prieto. 2003. Sphingomyelin/phosphatidylcholine/cholesterol phase diagram: boundaries and composition of lipid rafts. *Biophys. J.* 85:2406–2416.

31. Veatch, S. L., and S. L. Keller. 2005. Miscibility phase diagrams of giant vesicles containing sphingomyelin. *Phys. Rev. Lett.* 94:148101.

32. Boulgaropoulos, B., H. Amenitsch, …, G. Pabst. 2010. Implication of sphingomyelin/ceramide molar ratio on the biological activity of sphingomyelinase. *Biophys. J.* 99:499–506.

33. Bernstorff, S., H. Amenitsch, and P. Laggner. 1998. High-throughput asymmetric double-crystal monochromator of the SAXS beamline at ELETTRA. *J. Synchrotron Radiat.* 5:1215–1221.

34. Amenitsch, H., M. Rappolt, …, S. Bernstorff. 1998. First performance assessment of the small-angle X-ray scattering beamline at ELETTRA. *J. Synchrotron Radiat.* 5:506–508.

35. Spaar, A., and T. Salditt. 2003. Short range order of hydrocarbon chains in fluid phospholipid bilayers studied by x-ray diffraction from highly oriented membranes. *Biophys. J.* 85:1576–1584.

36. Podgornik, R., R. H. French, and V. A. Parsegian. 2006. Nonadditivity in van der Waals interactions within multilayers. *J. Chem. Phys.* 124: 044709.

37. Pabst, G., S. Danner, …, J. Katsaras. 2007. Entropy-driven softening of fluid lipid bilayers by alamethicin. *Langmuir.* 23:11705–11711.

38. Dan, N., and S. A. Safran. 1998. Effect of lipid characteristics on the structure of transmembrane proteins. *Biophys. J.* 75:1410–1414.

39. Cantor, R. S. 1999. Lipid composition and the lateral pressure profile in bilayers. *Biophys. J.* 76:2625–2639.

40. Cantor, R. S. 1999. The influence of membrane lateral pressures on simple geometric models of protein conformational equilibria. *Chem. Phys. Lipids.* 101:45–56.

41. Jerabek, H., G. Pabst, …, T. Stockner. 2010. Membrane-mediated effect on ion channels induced by the anesthetic drug ketamine. *J. Am. Chem. Soc.* 132:7990–7997.

42. Ben Shaul, A. 1995. Molecular theory of chain packing, elasticity and lipid-protein interaction in lipid bilayers. *In* Handbook of Biological Physics. R. Lipowsky and E. Sackmann, editors. Elsevier, Amterdam. 359–401.

43. Alley, S. H., O. Ces, …, R. H. Templer. 2008. X-ray diffraction measurement of the monolayer spontaneous curvature of dioleoylphosphatidylglycerol. *Chem. Phys. Lipids.* 154:64–67.

44. Mills, T. T., S. Tristram-Nagle, …, G. W. Feigenson. 2008. Liquid-liquid domains in bilayers detected by wide angle X-ray scattering. *Biophys. J.* 95:682–690.

45. Shah, J., J. M. Atienza, …, G. G. Shipley. 1995. Physical properties of ceramides: effect of fatty acid hydroxylation. *J. Lipid Res.* 36:1945–1955.

46. Chiu, S. W., E. Jakobsson, …, H. L. Scott. 2002. Cholesterol-induced modifications in lipid bilayers: a simulation study. *Biophys. J.* 83:1842–1853.

47. Maulik, P. R., P. K. Sripada, and G. G. Shipley. 1991. Structure and thermotropic properties of hydrated N-stearoyl sphingomyelin bilayer membranes. *Biochim. Biophys. Acta.* 1062:211–219.

48. Heberle, F. A., J. Wu, …, G. W. Feigenson. 2010. Comparison of three ternary lipid bilayer mixtures: FRET and ESR reveal nanodomains. *Biophys. J.* 99:3309–3318.

49. Pan, J., S. Tristram-Nagle, and J. F. Nagle. 2009. Effect of cholesterol on structural and mechanical properties of membranes depends on lipid chain saturation. *Phys. Rev. E.* 80:021931.

50. Popov, J., D. Vobornik, …, L. J. Johnston. 2008. Chemical mapping of ceramide distribution in sphingomyelin-rich domains in monolayers. *Langmuir.* 24:13502–13508.

51. Siegel, D. P. 2006. Determining the ratio of the Gaussian curvature and bending elastic moduli of phospholipids from Q(II) phase unit cell dimensions. *Biophys. J.* 91:608–618.

52. Chen, Z., and R. P. Rand. 1997. The influence of cholesterol on phospholipid membrane curvature and bending elasticity. *Biophys. J.* 73: 267–276.

53. Zimmerberg, J., and M. M. Kozlov. 2006. How proteins produce cellular membrane curvature. *Nat. Rev. Mol. Cell Biol.* 7:9–19.

54. Duesing, P. M., R. H. Templer, and J. M. Seddon. 1997. Quantifying packing frustration energy in inverse lyotropic mesophases. *Langmuir.* 13:351–359.

55. Kozlov, M. M., and M. Winterhalter. 1991. Elastic-moduli for strongly curved monolayers: position of the neutral surface. *J. Phys. II.* 1:1077–1084.

56. Rappolt, M. 2006. The biologically relevant lipid mesophases as "seen" by x-rays. *In* Advances in Planar Lipid Bilayers and Liposomes, *Vol. 5*. A. Leitmannova-Liu, editor. Elsevier, Amsterdam. 253–283.

57. Rand, R. P., N. L. Fuller, …, V. A. Parsegian. 1990. Membrane curvature, lipid segregation, and structural transitions for phospholipids under dual-solvent stress. *Biochemistry.* 29:76–87.

58. Feigenson, G. W. 2009. Phase diagrams and lipid domains in multicomponent lipid bilayer mixtures. *Biochim. Biophys. Acta.* 1788:47–52.

59. Wolff, J., C. M. Marques, and F. Thalmann. 2011. Thermodynamic approach to phase coexistence in ternary phospholipid-cholesterol mixtures. *Phys. Rev. Lett.* 106:128104.

60. Honerkamp-Smith, A. R., S. L. Veatch, and S. L. Keller. 2009. An introduction to critical points for biophysicists; observations of compositional heterogeneity in lipid membranes. *Biochim. Biophys. Acta.* 1788:53–63.